Available online at www.sciencedirect.com
SCIENCE DIRECT®
ELSEVIER
Journal of Power Sources 147 (2005) 227–233
JOURNAL OF POWER SOURCES
www.elsevier.com/locate/jpowsour

Improvement of silicon powder negative electrodes by copper electroless deposition for lithium secondary batteries

Jae Woo Kim, Ji Heon Ryu, Kyu T. Lee, Seung M. Oh *

School of Chemical Engineering and Research Center for Energy Conversion and Storage, Seoul National University, Seoul 151-744, Republic of Korea

Received 3 September 2004; accepted 28 December 2004
Available online 25 February 2005

Abstract

In order to enhance the electrical conductivity of Si powder, which shows a poor cycleabilty as the anode in lithium secondary batteries due to low electrical conductivity and a severe volume change on cycling, Cu is deposited on the Si surface by a electroless deposition method. As Cu deposition on bare Si powder is found to be unsatisfactory, Si powder is etched to roughen the surface, on to which a large amount of Cu deposit with a uniform coverage is obtained. The resulting anode material exhibits improved cycle performance as a result of conductivity enhancement. The long-term cycleability is, however, still unsatisfactory due to detachment of Cu from the Si surface that is caused by a severe volume change of the Si particles on cycling. The detachment of Cu is greatly suppressed by annealing at 400 °C in an inert atmosphere and, thereby, delivers better cycle performance. The improvement in interfacial stability exhibited by the annealed samples is ascribed to the formation of a Cu_3Si alloy phase at the interface and diffusion of Cu atoms into the Si particles.
© 2005 Elsevier B.V. All rights reserved.

Keywords: Lithium secondary battery; Silicon powder anode; Copper electroless deposition; Annealing; Galvanostatic intermittent titration; Cycle performance

1. Introduction

Recently, considerable attention has been paid to the use of Si, Al and Sn for the anode material in lithium secondary batteries since such electrodes possess higher theoretical specific capacity than that of graphite counterparts [1–6]. Among the three alternatives, Si has the highest theoretical specific capacity. The commercial use of Si powder is, however, still hindered because of two major problems. One is the low electrical conductivity of Si and the other is the volume expansion/contraction during the alloying and de-alloying reaction with Li^+ ions [7–14].

The failure modes in Si powder anode, which are closely related to the poor conductivity and severe volume change, have been reported by various workers [1–15]. In previous work [15], we found that Si particles are expanded upon charging as a result of the alloying reaction with Li^+ ions and electrons [15]. This behaviour leads to swelling of the electrode layer, in which carbon powder has been added to compensate for the poor conductivity of Si particles. During the discharge period, Si particles contract as a result of the de-alloying reaction, but the electrode layer still remains swollen because the electrode layer is not elastic. The net result after charge–discharge cycling is a breakdown of the conductive network between the Si and the carbon particles, which leads to an increase in the internal resistance. An abrupt increase in internal resistance causes an earlier approach to the discharge cut-off limit so that the de-alloying reaction is not completed and Si remains in a lithiated state. Upon a repeated cycling, Si anodes are degraded along with a successive accumulation of Li^+ ions inside the Si matrix. In summary, the failure modes of Si composite anodes are deeply associated with three features: (i) a severe volume change in Si particles upon cycling; (ii) a lack of elasticity of the electrode layer; (iii) poor conductivity of the Si and lithiated Si particles.

One way to solve the above problems is enhancement of the electrical conductivity of Si particles by coating with con-

* Corresponding author. Tel.: +82 2 880 7074; fax: +82 2 888 1604.
E-mail address: seungoh@plaza.snu.ac.kr (S.M. Oh).

0378-7753/$ – see front matter © 2005 Elsevier B.V. All rights reserved.
doi:10.1016/j.jpowsour.2004.12.041

ductive materials. This is because, it is expected that the internal resistance will not be very high since the conductive surface layer reduces the contact and charge-transfer resistances even if the conductive network is broken. With this expectation in mind, we have deposited Cu on the surface of Si particles by electroless deposition. To achieve a uniform/strong Cu deposition, etching of the Si powder and annealing of the Cu-deposited Si have been performed. The material characteristics and anodic performance of Cu-deposited Si powder anodes have been examined and are reported in this communication.

2. Experimental

2.1. Materials

The Cu-deposited Si powders were prepared via the following three steps: (i) etching Si powder to enhance the surface roughness [16,17]; (ii) electroless deposition [18,19]; (iii) annealing the Cu-deposited Si powder to improve the interfacial stability. In order to etch the Si powder, commercially available Si powder (Aldrich Chem. Co., 325 mesh, 99%) was dispersed in an etching solution that consisted of 49 wt.% hydrofluoric acid, 60 wt.% nitric acid and de-ionized water (1:5:10 in volume ratio). After mild stirring for 4 min, the solution was poured into a large amount of de-ionized water to stop the etching reaction. After a filtration, the etched Si powder was dispersed in a hydrofluoric acid solution that contained copper sulfate (Kanto Chem. Co., 99%) to perform the electroless deposition. The resulting Cu-deposited Si powder was filtered and rinsed with de-ionized water to remove the residual solution, and then dried in a vacuum oven at 80 °C for 12 h. The amount of Cu deposit was controlled by the Cu^{2+} concentration (4–10 mM) and deposition time (15 min–3 h). The Cu-deposited Si powder was annealed at 400–800 °C for 9 h under an argon atmosphere.

Field-emission scanning electron microscope (FE-SEM) images were obtained with a JEOL JSM-6700F. X-ray powder diffraction (XRD) analysis and Auger electron spectroscopy (AES) depth-profiling were performed with a MAC Science Co. M18XHF-SRA with Cu Kα radiation and a Perkin-Elmer model 660, respectively. In the depth-profiling experiment, the penetration depth was estimated by assuming that the sputter rate (40 nm min^{-1}) obtained for a SiO_2 reference sample at the same accelerating voltage is similar to that for the present samples. The electrical conductivity of powder samples was measured by means of the four-probe Van der Pauw method under a constant pressure (0.5 ton cm^{-2}) [20].

2.2. Electrochemical characterization

To prepare the Si composite anodes, a mixture of Si powder, Super P (carbon additive for conductivity enhancement) and poly(vinylidene fluoride) (PVdF as a binder) (5:2:1.5 in weight ratio) was dispersed in *N*-methyl pyrrolidone (NMP) and homogenized for 2 h. The resulting slurry was spread on a piece of copper foil (current collector, thickness = 25 μm and apparent area = 1 cm^2) and dried in vacuum at 120 °C for 12 h. The electrode was roll-pressed in order to enhance the inter-particle contact and to ensure better adhesion to the current-collector.

Half-cell characteristics were analyzed in a beaker-type three-electrode cell, in which lithium foil (Cyprus Co.) was used for both the counter and reference electrodes. The electrolyte was 1.0 M $LiClO_4$ in ethylene carbonate (EC)/diethyl carbonate (DEC) (1:1 volume ratio). Galvanostatic charge–discharge cycling was performed with a gravimetric current density of 100 mA g^{-1} over the voltage range of 0.0 to 2.0 V (versus Li/Li^+). The galvanostatic intermittent titration technique (GITT) [21] was employed to monitor the evolution of internal resistance during cycling, where a current pulse of 100 mA g^{-1} was applied for 10 min to measure the close-circuit voltage (CCV) and turned off for 20 min to obtain the quasi-open-circuit voltage (QOCV). The sequential current pulse was applied for both the charging and the discharging periods in the range of 0.0–2.0 V. The internal resistance was calculated from the difference between the CCV and QOCV in each voltage transient. All the electrochemical measurements were made with a WBCS-3000 battery cycler (Xeno Co.) at ambient temperature in a glove-box that was filled with argon.

3. Results and discussion

3.1. Material characterization

The properties of the Cu-deposited Si powder samples prepared in this work, are listed in Table 1 in terms of the Cu/Si weight ratio, annealing temperature and electrical conductivity. The first two samples were made from the bare Si powder, whereas the other eight samples were produced from etched powder.

Table 1
Electrical conductivity of Cu-deposited Si powders according to Cu:Si ratio and annealing temperature

	Cu:Si (weight ratio)	Annealing temperature (°C)	Electrical conductivity (S cm^{-1})
Bare Si			
Sample 1	0	–	0.02
Sample 2	0.05	–	0.15
Etched Si			
Sample 3		–	190
Sample 4	0.19	400	18.1
Sample 5		600	5.7
Sample 6		800	1.3
Sample 7	0.47	–	247
Sample 8		400	240
Sample 9	1.10	–	280
Sample 10		400	276

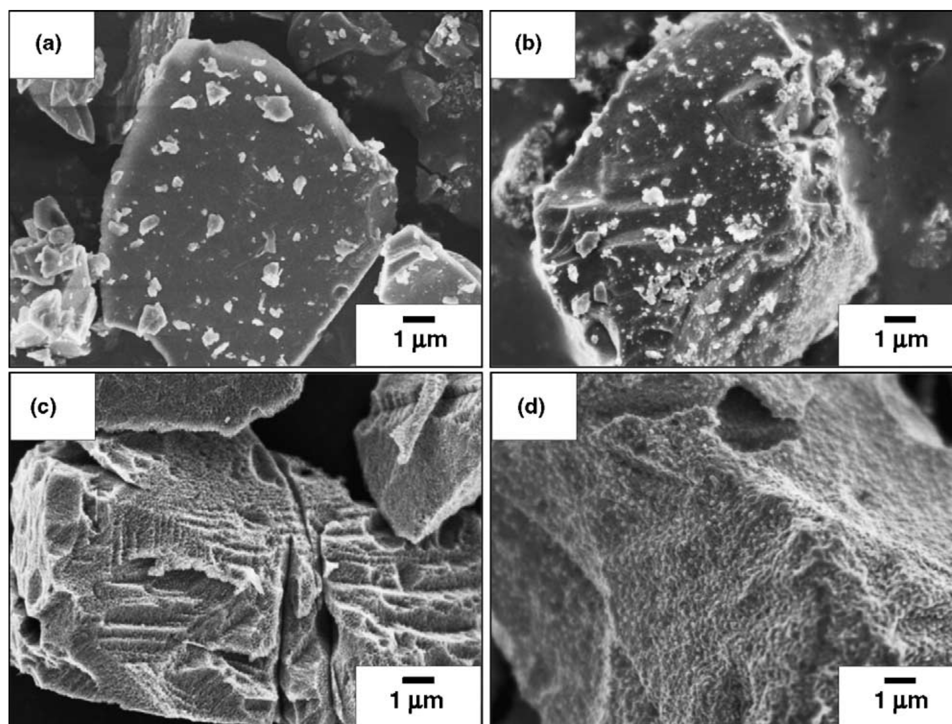

Fig. 1. Field-emission scanning electron microscope (FE-SEM) images of: (a) bare Si (sample 1); (b) Cu-deposited bare Si (sample 2); (c) etched Si; (d) Cu-deposited etched Si (sample 3).

Typical FE-SEM images of Si powder and Cu-deposited samples are shown in Fig. 1. The average particle size of bare Si powder is about 10 μm (Fig. 1(a)). Cu electroless deposition on to bare Si is not satisfactory in that the amount of Cu deposit is very small (Fig. 1(b)) and is easily detached even during the washing period. The surface morphology of etched Si particles, presented in (Fig. 1(c)). The roughened Si surface with a high population of thorn-like tips is read-

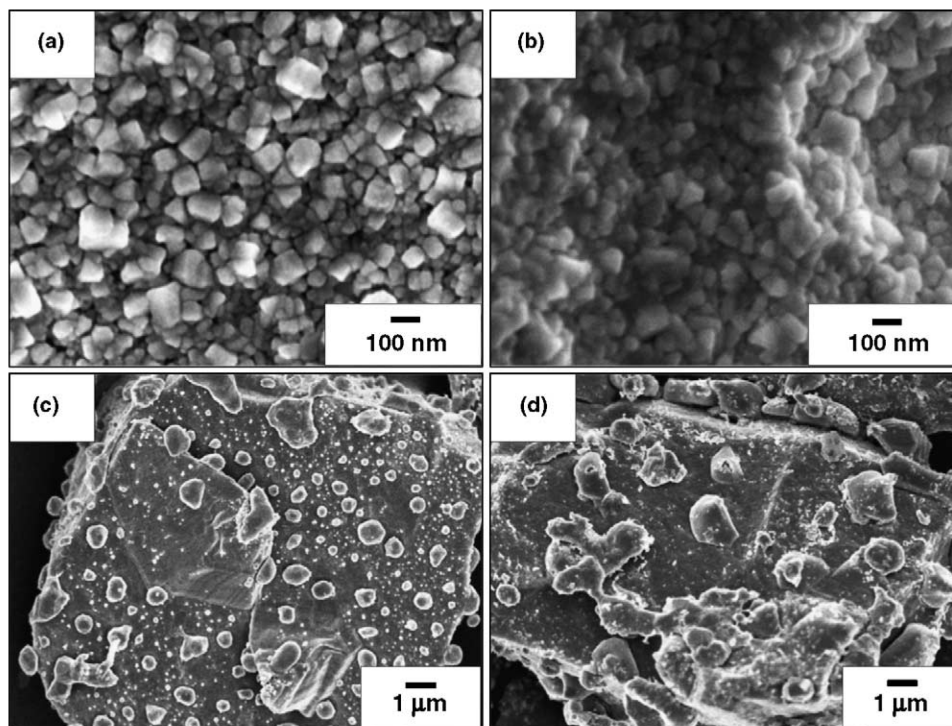

Fig. 2. Field-emission scanning electron microscope (FE-SEM) images of Cu-deposited Si powders (Cu:Si = 0.19): (a) as-deposited (sample 3); (b) annealed at 400 °C (sample 4); (c) annealed at 600 °C (sample 5); (d) annealed at 800 °C (sample 6).

ily discernible [17,22]. Electroless deposition on the etched Si surface is greatly facilitated due to the large surface area and sharp tips, and thereby gives rise to a larger amount of Cu deposit with a uniform surface coverage (Fig. 1(d)). The size of the Cu deposit is about 100 nm, as seen in the magnified view given in (Fig. 2(a)). Annealing at 400 °C does not affect the morphology of the Cu deposit (Fig. 2(b)). The particle size of the Cu deposit remains the same and the porous Cu layer for ion penetration is still maintained. Annealing at higher temperature (600 and 800 °C), however, leads to extensive Cu aggregation, so that the resulting lump-shaped Cu deposit does not cover the whole Si surface (Fig. 2(c) and (d)). Based on this observation, the annealing temperature is fixed at 400 °C in further experiments.

The X-ray diffraction patterns of samples 3–6 are given in Fig. 3. The samples differ in the annealing temperature, while the Cu:Si ratio (0.19) is the same. The Cu-deposited Si powders display diffraction peaks that belong to the Cu_2O phase, as well as peaks for Cu and Si. The former is seemingly formed during the electroless deposition period [18]. With annealing, however, additional peaks at 45° develop with an intensity that becomes higher with increase in annealing temperature. The 45° peaks can be indexed as those for Cu_3Si alloy phase [23,24]. Auger electron spectroscopy (AES) depth-profiling data taken before and after annealing at 400 °C are displayed in Fig. 4. The oxygen at the outermost surface region comes from the Cu_2O phase, whereas the additional oxygen population results from the SiO_2 layer on the Si surface (Fig. 4(a)). Annealing leads to intensive Cu diffusion into the Si particles (Fig. 4(b)) [23]. Based on the point where the Cu concentration is 10 wt.%, the thickness of Cu diffusion layer is estimated to be 140 and 340 nm before and after the annealing, respectively.

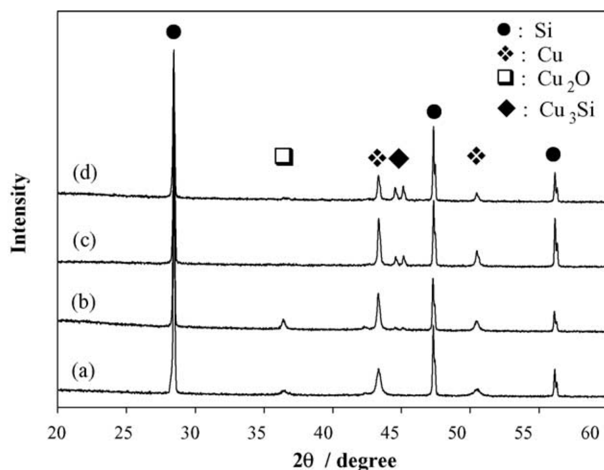

Fig. 3. X-ray diffraction (XRD) patterns of Cu-deposited Si powders (Cu:Si = 0.19): (a) as-deposited (sample 3); (b) annealed at 400 °C (sample 4); (c) annealed at 600 °C (sample 5); (d) annealed at 800 °C (sample 6).

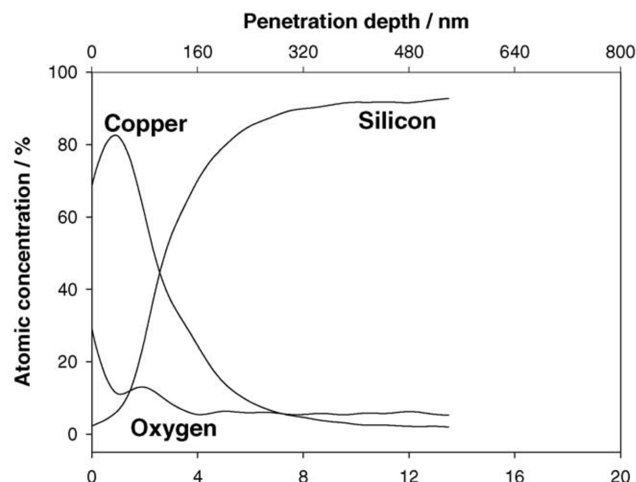

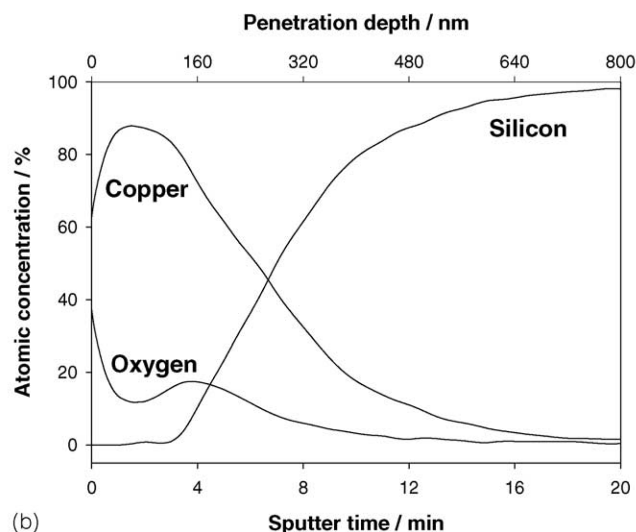

Fig. 4. Auger electron spectroscopy (AES) depth profiles of Cu-deposited Si powders (Cu:Si = 0.19): (a) as deposited (sample 3); (b) annealed at 400 °C (sample 4).

3.2. Electrochemical measurements

Galvanostatic charge–discharge voltage profiles for samples 1 and 10 are shown in Fig. 5. The bare Si powder (sample 1) electrode delivers a specific discharge capacity of 880 mAh g^{-1} on the first cycle even if the charging capacity is as high as 3700 mAh g^{-1}. This anode degrades within a few cycles and has been reported in our previous investigation [15]. Sample 10, which was annealed at 400 °C after Cu deposition, exhibits improved cycleability. The first charging capacity of this anode is, however, smaller than that of bare Si because Cu is not active for the Li alloying reaction. One apparent feature in both profiles is that the irreversible capacity results from electrolyte decomposition and concomitant formation of a solid electrolyte interface (SEI) during the first charging (alloying) period is negligible. This is somewhat unusual given that graphite anodes always exhibit a voltage plateau near 0.8–1.0 V (versus

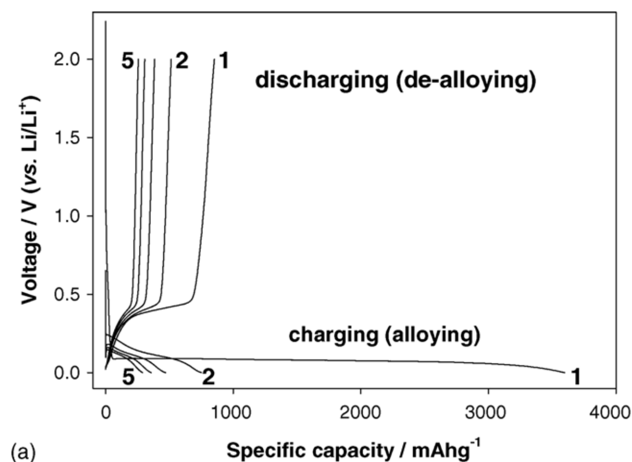

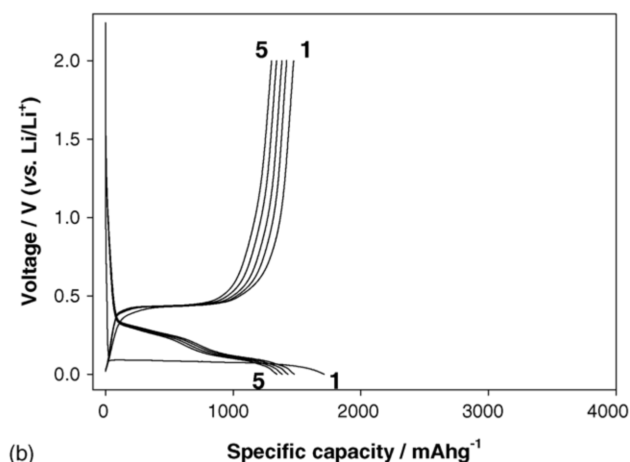

Fig. 5. Galvanostatic charge–discharge voltage profiles of: (a) sample 1; (b) sample 10. A gravimetric current density of 100 mA g^{-1} is applied over the voltage range of 0.0–2.0 V (vs. Li/Li^+).

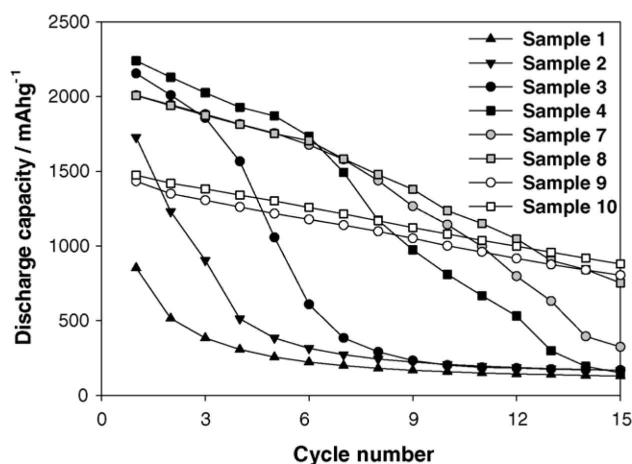

Fig. 6. Specific discharge capacity of samples 1–4 and 7–10 according to cycle number.

Li/Li^+) as a result of SEI formation [25]. The absence of SEI formation in Si anodes has been reported [9,26] and attributed to the fact that electrolyte decomposition is greatly reduced due to the presence of an oxide layer on the Si surface [9,26].

The discharge capacity profiles of all the samples are given in Fig. 6. Two decisive factors appear to control the cycleability of Si powder anodes. One is the electrical conductivity of Si powders. A comparison of the cycleability data for samples 1–3, which have different electrical conductivities, reveals that the first discharge capacity is larger and that the capacity retention over a few cycles becomes better with increase in the conductivity of Si powders. In particular, it is noticeable that the first specific discharge capacity of Cu-deposited Si (sample 3) is much higher than that of bare Si (sample 1), even if the former contains inactive Cu. This improvement can be attributed to the presence of a conductive surface layer on the Si particles. That is, even when the Si particles contract during the discharging period after swelling of the electrode layer during the preceding charging period, the conductive Cu deposit can still provide an electron transfer channel. As a result, the contact resistance and the charge-transfer resistance for the de-alloying reaction are lowered and the de-alloying reaction can be continued. This feature has been confirmed by galvanostatic intermittent titration experiments. A typical transient voltage profile is presented in Fig. 7(a) along with the voltage transient observed during one current pulse cycle (see inset). The voltage transient comprises a rapid fall in voltage in the initial period due to the ohmic resistance, but a rather slow decay in the later stage due to the charge-transfer resistance. When the current pulse is turned off, however, voltage is restored to the initial quasi-equilibrium value. The uppermost trace in the charging profile in Fig. 7(a) thus corresponds to the QOCV and the bottom to the CCV. Conversely, the uppermost trace in the discharging period represents the CCV. The internal resistance was calculated from the difference between QOCV and CCV in each voltage transient; the results are presented in Fig. 7(b). One apparent feature in Fig. 7(b) is that all the samples exhibit a steady decrease in internal resistance during the charging period, which has been ascribed in our previous report [27] to either a better contact between Si and carbon particles due to a volume expansion in the Si particles themselves, or a slightly higher electrical conductivity of lithiated Si. In the discharging period, however, the samples show a different behaviour according to the method of their preparation. The bare Si anode (sample 1) shows an abrupt increase in internal resistance near 0.4 V, whereas the increase in internal resistance is much slower for Cu-deposited Si electrodes.

Careful inspection of the conductivity data (Table 1) and the cycleability in Fig. 6 reveals that the conductivity enhancement induced by Cu deposition cannot explain fully the improvement in cycleability. For instance, the annealed Cu-deposited Si anode (sample 4) exhibits better capacity retention than the un-annealed counterpart (sample 3), even through its conductivity is one order of magnitude smaller. A similar disagreement between conductivity and cycleabilty

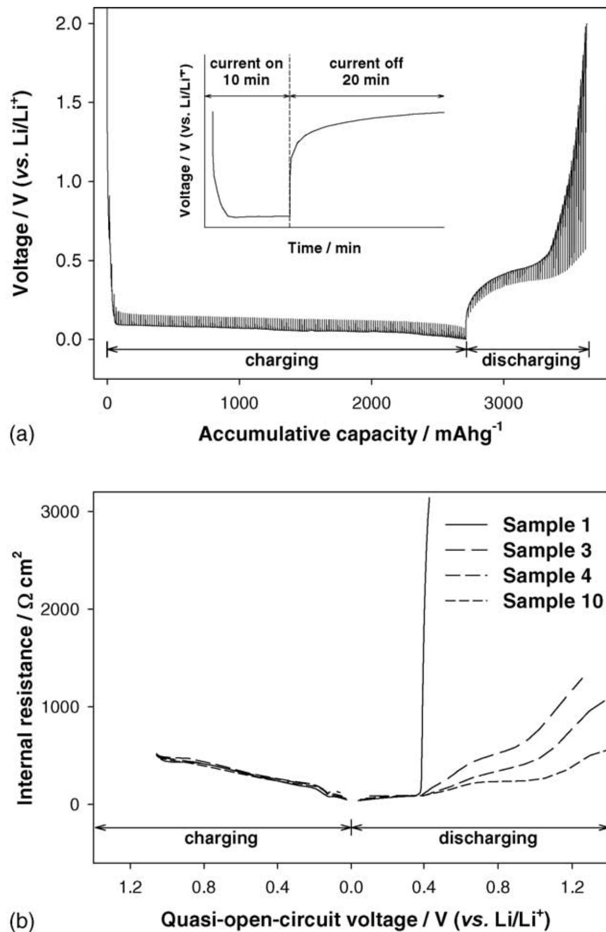

Fig. 7. (a) Transient voltage profiles of sample 1 obtained with the galvanostatic intermittent titration technique (GITT). A typical voltage transient for one current pulse cycle is represented in the inset; (b) evolution of internal resistance traced with sample 1, 3, 4, and 10 electrodes.

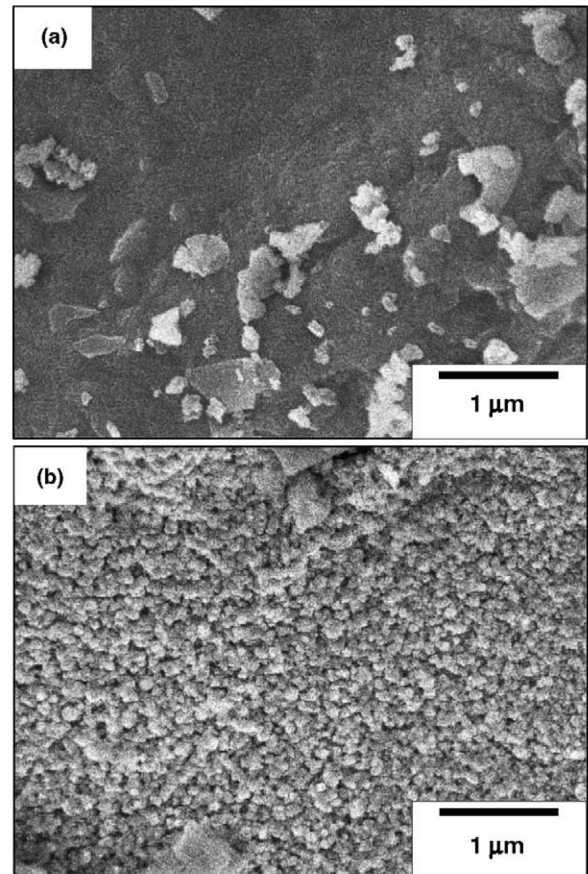

Fig. 8. Field-emission scanning electron microscope (FE-SEM) images of Cu-deposited Si powder anodes (Cu:Si = 0.19) taken after three cycles: (a) sample 3 (un-annealed); (b) sample 4 (annealed at 400 °C for 9 h).

can be identified between samples 7 and 8, and between 9 and 10. The poorer conductivity observed with the annealed powder samples may be ascribed to the formation of Cu_3Si alloy phase on the Si surface. Note that, the Cu_3Si alloy phase has a lower conductivity than pure Cu [28].

The increased-performance of annealed samples over un-annealed ones can be explained by comparing scanning electron micrographs of samples 3 and 4 that were taken after three cycles (Fig. 8). The annealed Si powder still has the Cu deposit on its surface even after three cycles (Fig. 8(b)), whereas severe detachment of Cu from the Si surface, which is seemingly caused by the volume change in the Si particles themselves, takes place in the un-annealed powder (Fig. 8(a)). This result strongly suggests that annealing imparts greater stability to the Cu deposit and that the interfacial stability plays a key role in controlling the cycleability. Because the Cu deposit is detached upon cycling, the Cu deposit in the un-annealed powder cannot provide an electronic pathway between the Si and carbon particles. In the case of the annealed powders, however, even if their conductivity is lower than that of the un-annealed one in the powder state, the Cu deposit is still adheres well to the Si surface and provides an electronic channel. This feature is further ascertained from the data shown in Fig. 7(b), where it is seen that the increase in internal resistance is slower with annealed samples (samples 4 and 10).

The electrical conductivity of heavily deposited samples (7–10) is listed in Table 1, and their cycleability and variation of internal resistance is presented in Figs. 6 and 7(b), respectively. As shown in Table 1, the conductivity of the Cu-deposited Si powders increases with increase in the Cu:Si ratio. The fall in conductivity caused by annealing becomes less significant in the heavily deposited ones. This can be explained by the fact that the outermost surface region of Si powder is still covered by the Cu deposit even if some fraction of Cu is converted to the Cu_3Si alloy during the annealing period. In two sets of heavily deposited Si powders (Cu:Si = 0.47 for samples 7 and 8, and = 1.10 for samples 9 and 10), better cycleability is observed with the more conductive powders and the annealing effect prevails by delivering an improved cycle performance. Electron micrographs taken after three cycles reveal that the detachment of Cu is was insignificant in the heavily deposited samples.

4. Conclusions

In this work, Cu electroless deposition is performed to enhance the electrical conductivity of Si powder. Etching and annealing steps were added before and after the electroless deposition. The resulting Cu-deposited Si powder negative electrodes exhibit improved cycleability compared with base Si anodes. The following observations has been made:

(i) A greater amount of Cu deposit with a uniform coverage is obtained by etching the Si surface.
(ii) A uniform coverage of the porous Cu layer for ion penetration is maintained even after annealing at 400 °C. When annealed at a higher temperature, however, the deposit does not cover the whole Si surface due to extensive aggregation of the Cu.
(iii) Cu-deposited Si powder anodes deliver better capacity retention than bare Si, which can be ascribed to conductivity enhancement. The interfacial stability of the Cu deposit, however, is found to be the more important factor in controlling the cycle performance. Annealed samples display better cycleability than un-annealed ones, despite the fact that their electrical conductivity is lower. The detachment of Cu from the Si surface upon cycling is less significant in annealed samples. The interfacial stability is likely provided by the formation of a Cu_3Si phase at the interface and Cu diffusion into the Si particles.

Acknowledgements

This work was partially supported by KOSEF through the Research Center for Energy Conversion and Storage, and by financial support from the Center for Nanostructured Materials Technology under the 21st Century Frontier R&D Programs of the Ministry of Science and Technology, Korea. Financial support from LG Chem. Ltd. is also acknowledged.

References

[1] M. Winter, J.O. Besenhard, M.E. Spahr, P. Novak, Adv. Mater. 10 (1998) 725.
[2] P. Poizot, S. Laruelle, S. Grugeon, L. Dupont, J.-M. Tarascon, Nature 40 (2000) 496.
[3] Y. Idota, T. Kubota, A. Matsufuji, Y. Maekawa, T. Muyasaka, Science 276 (1997) 1395.
[4] M. Winter, J.O. Besenhard, Electrochim. Acta 45 (1999) 31.
[5] J.O. Besenhard, J. Yang, M. Winter, J. Power Sources 68 (1997) 87.
[6] M. Wachtler, M. Winter, J.O. Besenhard, J. Power Sources 105 (2002) 151.
[7] A.M. Wilson, J.R. Dahn, J. Electrochem. Soc. 142 (1995) 326.
[8] H. Li, X. Huang, L. Chen, Z. Wu, Y. Liang, Electrochem. Solid-State Lett. 2 (1999) 547.
[9] H. Li, X. Huang, L. Chen, G. Zhou, Z. Zhang, D. Yu, Y.J. Mo, N. Pei, Solid State Ionics 135 (2000) 181.
[10] M. Yoshio, H. Wang, K. Fukuda, T. Umeno, N. Dimov, Z. Ogumi, J. Electrochem. Soc. 149 (2002) A1598.
[11] N. Dimov, K. Fukuda, T. Umeno, S. Kugino, M. Yoshio, J. Power Sources 114 (2003) 88.
[12] J. Yang, B.F. Wang, K. Wang, Y. Liu, J.Y. Xie, Z.S. Wen, Electrochem. Solid-State Lett. 6 (2003) 154.
[13] J. Niu, J.Y. Lee, Electrochem. Solid-State Lett. 5 (2002) A107.
[14] A.M. Wilson, J.N. Reimers, E.W. Fuller, J.R. Dahn, Solid State Ionics 74 (1994) 249.
[15] J.H. Ryu, J.W. Kim, Y.E. Sung, S.M. Oh, Electrochem. Solid-State Lett. 7 (2004) A306.
[16] S. Shih, K.H. Jung, T.Y. Hsieh, J. Sarathy, J.C. Campbell, D.L. Kwong, Appl. Phys. Lett. 60 (1992) 1863.
[17] D. Dimova-Malinovska, M. Sendova-Vassileva, N. Tzenov, M. Kamenova, Thin Solid Films 297 (1997) 9.
[18] H. Morinaga, M. Suyama, T. Ohmi, J. Electrochem. Soc. 141 (1994) 2834.
[19] Y. Shacham-Diamand, S. Lopatin, Electrochim. Acta 44 (1999) 3639.
[20] L.J. van der Pauw, Philips Tech. Rev. 20 (1958) 220.
[21] C.J. Wen, B.A. Boukamp, R.A. Huggins, W. Weppner, J. Electrochem. Soc. 126 (1979) 2258.
[22] X. Li, P.W. Bohn, Appl. Phys. Lett. 77 (2000) 2572.
[23] C.Y. Yang, J.S. Jeng, J.S. Chen, Thin Solid Films 420–421 (2002) 398.
[24] J.T. No, J.H. O, C.M. Lee, Mater. Chem. Phys. 63 (2000) 44.
[25] S. Flandrois, B. Simon, Carbon 37 (1999) 165.
[26] X.D. Wu, Z.X. Wang, L.Q. Chen, X.J. Huang, Electrochem. Commun. 5 (2003) 935.
[27] L.A. Stearns, J. Gryko, J. Diefenbacher, G.K. Ramachandran, P.F. McMillan, J. Solid State Chem. 173 (2003) 251.
[28] C. Rong, J. Zhang, W. Li, Appl. Surf. Sci. 220 (2003) 40.